

CrossMark
click for updatesCite this: *Chem. Sci.*, 2015, 6, 3063

Unexpected effect of catalyst concentration on photochemical CO₂ reduction by *trans*(Cl)–Ru(bpy)(CO)₂Cl₂: new mechanistic insight into the CO/HCOO[–] selectivity†

Yusuke Kuramochi,^a Jun Itabashi,^a Kyohei Fukaya,^a Akito Enomoto,^a Makoto Yoshida^a and Hitoshi Ishida^{*ab}

Photochemical CO₂ reduction catalysed by *trans*(Cl)–Ru(bpy)(CO)₂Cl₂ (bpy = 2,2′-bipyridine) efficiently produces carbon monoxide (CO) and formate (HCOO[–]) in *N,N*-dimethylacetamide (DMA)/water containing [Ru(bpy)₃]²⁺ as a photosensitizer and 1-benzyl-1,4-dihydronicotinamide (BNAH) as an electron donor. We have unexpectedly found catalyst concentration dependence of the product ratio (CO/HCOO[–]) in the photochemical CO₂ reduction: the ratio of CO/HCOO[–] decreases with increasing catalyst concentration. The result has led us to propose a new mechanism in which HCOO[–] is selectively produced by the formation of a Ru(I)–Ru(I) dimer as the catalyst intermediate. This reaction mechanism predicts that the Ru–Ru bond dissociates in the reaction of the dimer with CO₂, and that the insufficient electron supply to the catalyst results in the dominant formation of HCOO[–]. The proposed mechanism is supported by the result that the time-course profiles of CO and HCOO[–] in the photochemical CO₂ reduction catalysed by [Ru(bpy)(CO)₂Cl₂] (0.05 mM) are very similar to those of the reduction catalysed by *trans*(Cl)–Ru(bpy)(CO)₂Cl₂ (0.10 mM), and that HCOO[–] formation becomes dominant under low-intensity light. The kinetic analyses based on the proposed mechanism could excellently reproduce the unusual catalyst concentration effect on the product ratio. The catalyst concentration effect observed in the photochemical CO₂ reduction using [Ru(4dmbpy)₃]²⁺ (4dmbpy = 4,4′-dimethyl-2,2′-bipyridine) instead of [Ru(bpy)₃]²⁺ as the photosensitizer is also explained with the kinetic analyses, reflecting the smaller quenching rate constant of excited [Ru(4dmbpy)₃]²⁺ by BNAH than that of excited [Ru(bpy)₃]²⁺. We have further synthesized *trans*(Cl)–Ru(6Mes-bpy)(CO)₂Cl₂ (6Mes-bpy = 6,6′-dimesityl-2,2′-bipyridine), which bears bulky substituents at the 6,6′-positions in the 2,2′-bipyridyl ligand, so that the ruthenium complex cannot form the dimer due to the steric hindrance. We have found that this ruthenium complex selectively produces CO, which strongly supports the catalytic mechanism proposed in this work.

Received 19th January 2015
Accepted 3rd March 2015

DOI: 10.1039/c5sc00199d

www.rsc.org/chemicalscience

Introduction

Photocatalytic CO₂ reduction represents a major concern in relation to the construction of artificial photosynthetic systems and solar fuels, which are relevant to the solution of the fossil fuel shortage and the global warming problems.^{1–4} Until now, many metal complexes have been investigated for CO₂ reduction catalysis.^{5–15} As metal complexes for the catalysts, manganese mono(bipyridyl) tricarbonyl,^{16–18} cobalt and iron porphyrin,^{19–21} cobalt

tris(bipyridyl)²² and macrocycle,^{23,24} nickel cyclam,^{25–27} molybdenum and tungsten mono(bipyridyl) tetracarbonyl,²⁸ rhodium bis(bipyridyl),^{29,30} palladium phosphine,^{31–33} rhenium mono(bipyridyl) tricarbonyl,^{34–42} osmium mono(bipyridyl) dicarbonyl,^{43,44} iridium poly(pyridyl) and dihydride pincer,^{45,46} ruthenium mono(bipyridyl) and bis(bipyridyl) dicarbonyl complexes^{47–70} have been investigated. Most of these yield CO and/or formate as the two-electron reduction products of CO₂. Among the metal complex catalysts, ruthenium complexes (*e.g.*, [Ru(bpy)₂(CO)₂]²⁺) have actively been studied for the CO/HCOO[–] selectivity. In the catalyses, the product selectivity depends on the reaction conditions: acidic conditions enhance CO production while basic conditions cause formate production.^{51–56,69} Photochemical reductions have mostly resulted in formate production^{47–49,51–53,57–62,70} while electrochemical reductions have achieved the selective formation of CO.^{55,63–69} The reaction mechanisms of

^aDepartment of Chemistry, Graduate School of Science, Kitasato University, 1-15-1 Kitasato, Minami-ku, Sagami-hara, Kanagawa 252-0373, Japan. E-mail: ishida@sci.kitasato-u.ac.jp

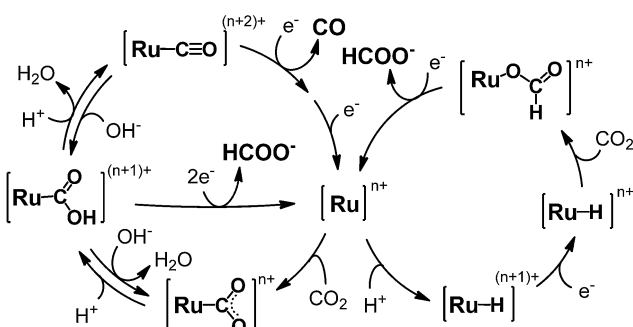
^bPrecursory Research for Embryonic Science (PRESTO), Japan Science and Technology Agency (JST), 4-1-8 Honcho, Kawaguchi, Saitama, 332-0012, Japan

† Electronic supplementary information (ESI) available. See DOI: 10.1039/c5sc00199d



Ru(II) complexes have been proposed as shown in Scheme 1.^{50–56,69} The widely accepted mechanism of CO production is as follows: (1) the Ru(II) complex accepts one electron to release CO, (2) the one-electron-reduced complex accepts another electron, and (3) the two-electron-reduced complex undergoes an electrophilic attack by CO₂ along with protonation and dehydration to regenerate the starting Ru(II) complex. For formate production, two mechanisms have been proposed so far. Tanaka and co-authors have proposed a mechanism in which the equilibrium between [Ru–C(O)OH]⁽ⁿ⁺¹⁾⁺ and [Ru–CO]⁽ⁿ⁺²⁾⁺ governs the product selectivity between CO/HCOO[–]: the two-electron reduction of [Ru–C(O)OH]⁽ⁿ⁺¹⁾⁺ causes formate production.^{51–56,69} This mechanism can explain well that formate is mainly produced under basic conditions where the equilibrium shifts to the hydroxycarbonyl complex. However, it is not fully accepted because the reaction requires a specific proton attack on the carbon atom of the hydroxycarbonyl group. Meyer *et al.* have proposed that formate is generated *via* insertion of CO₂ into the Ru–H bond in [Ru–H]ⁿ⁺.⁵⁰ The mechanism *via* the hydride complex is based on the experimental result that [Ru(bpy)₂(CO)H]⁰ reacts with CO₂ to yield [Ru(bpy)₂(CO)(OC(O)H)]⁰, and is generally accepted as the mechanism of formate production in organometallic chemistry. However, this mechanism does not successfully elucidate why formate is selectively produced under less protic conditions and why dihydrogen originating from the hydride intermediate scarcely evolves when formate is produced, but does evolve with CO production. Even today with more than 20 years having passed since these mechanisms were proposed, consensus on the reaction mechanism of formate production has not yet been reached.

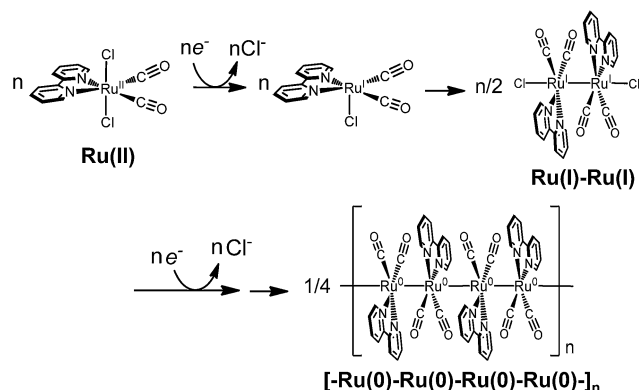
Recently, polymeric ruthenium mono(bipyridyl) dicarbonyl complexes (*e.g.*, [Ru(L)(CO)₂]_n (L = bipyridyl derivatives)) have been utilized as reduction catalysts in artificial photosynthetic systems using semiconductors, which can utilize water as an electron donor.⁶⁰ The system consists of TiO₂ and InP modified with the ruthenium polymer. Photo-irradiation of the system induces electron transfer from the semiconductors to the ruthenium polymer, which catalyses CO₂ reduction using the electrons to afford formate in a 10 mM NaHCO₃ aqueous solution with CO₂ bubbling. Polymeric ruthenium mono(bipyridyl) dicarbonyl complexes have been reported as catalysts in electrochemical CO₂ reduction by Deronzier and Ziesel *et al.*^{63–65,67,68} The selectivity of CO *vs.* formate production depends essentially



Scheme 1 Combined mechanisms⁴⁸ proposed by Tanaka *et al.*⁶⁹ and Meyer *et al.*⁵⁰

on the substituents which are introduced at the 4,4' position of the bipyridyl ligand in aqueous solution.⁶⁴ Ruthenium mono(bipyridyl) dicarbonyl polymers and their derivatives with electron-donating substituents give mainly CO as the reduction product at pH 6. The pH values of the solution and the electrolytes (*e.g.*, NaSO₄ *vs.* LiClO₄) used for the electrolyses moderately affect the selectivity. On the contrary, polymer complexes with electron-withdrawing substituents quantitatively yield HCOO[–]. This difference is explained by the electronic structures of the catalyst intermediates (the hydroxycarbonyl or formato complexes) formed during the electrocatalytic process. A similar tendency has been reported for electrocatalyses by derivatives of [Ru(bpy)₂(CO)₂]²⁺.⁶⁹ Thus, results in the literature indicate that the reaction mechanisms and the product selectivity strongly depend on the reaction conditions. However, to the best of our knowledge, there is no report on the effects of catalyst concentration on product selectivity in CO₂ reduction.

The polymeric ruthenium mono(bipyridyl) dicarbonyl complexes are obtained by electrochemical reductions of mono(bipyridyl) dicarbonyl dichloride complexes,^{63–65,67,68,71,72} as well as ruthenium bis(bipyridyl) dicarbonyl complexes.⁶⁶ For instance, the formation process of [Ru(bpy)(CO)₂]_n is shown in Scheme 2. The electrochemical reduction of Ru(bpy)(CO)₂Cl₂ initially dissociates the chloride ion to form a dimer, [Ru(bpy)(CO)₂Cl]₂, which has already been elucidated by Haukka *et al.* with X-ray crystallographic analysis.⁷³ Further reduction of the ruthenium dimer causes dissociation of the chloride ions to give [Ru(bpy)(CO)₂]_n. The monomeric ruthenium complex, Ru(bpy)(CO)₂Cl₂, also shows catalytic activity for electrochemical CO₂ reduction,^{63,65,67,69} but the complex tends to form an adherent film of the polymer on the electrode during electrochemical CO₂ reduction, making it difficult to investigate the catalytic properties of the monomeric complex in detail. The photochemical CO₂ reduction catalysed by Ru(bpy)(CO)₂Cl₂ has been reported in the presence of [Ru(bpy)₃]²⁺ as the photosensitizer and triethanolamine (TEOA) as the electron donor,⁷⁰ in which the reaction starts when [Ru(bpy)₃]²⁺ absorbs visible light to induce electron transfer relay from TEOA to the catalyst. However, the system also causes the polymeric complex to form a black precipitate during the catalytic reaction, which probably



Scheme 2 Formation of the polymeric ruthenium complex from *trans*(Cl)–Ru(bpy)(CO)₂Cl₂.



inhibits light absorption and/or electron transfer from the photosensitizer.

We have very recently reported photochemical CO₂ reduction catalysed by [Ru(bpy)₂(CO)₂]²⁺ in *N,N*-dimethylacetamide (DMA)/water containing [Ru(bpy)₃]²⁺ and 1-benzyl-1,4-dihydronicotinamide (BNAH).⁴⁷ DMA is used as an alternative solvent for *N,N*-dimethylformamide (DMF), which is the most frequently used solvent in photochemical CO₂ reduction, but has been indicated to cause contamination of HCOO⁻ by hydrolysis.⁷⁴ In the DMA/water systems using BNAH as the electron donor, the black precipitate scarcely formed, and the photocatalytic CO₂ reduction proceeded smoothly. The products were CO and formate, which were confirmed as the CO₂ reduction products by the ¹³C NMR experiments. We further showed that the oxidized form of BNAH was the BNA dimer, *e.g.*, 1,1'-dibenzyl-1,1',4,4'-tetrahydro-4,4'-bincotinamide (4,4'-BNA₂),^{47,49} indicating that the reduced species of the photosensitizer ([Ru(bpy)₃]⁺), which was generated by the reductive quenching of the excited [Ru(bpy)₃]²⁺ with BNAH, supplied the electrons to the catalyst.

In this work, we have investigated photochemical CO₂ reduction catalysed by *trans*(Cl)-Ru(bpy)(CO)₂Cl₂ in a DMA/water solution containing [Ru(bpy)₃]²⁺ and BNAH (Fig. 1). We have unexpectedly discovered that the concentration of *trans*(Cl)-Ru(bpy)(CO)₂Cl₂ affects the product selectivity (CO/HCOO⁻). The mechanisms reported so far^{48,50–56,64,69,70} cannot explain the phenomenon. This motivated us to reconsider the reaction mechanism of photochemical CO₂ reduction. We propose a new reaction mechanism involving a Ru(I)-Ru(I) dimer, which catalyses CO₂ reduction to selectively produce formate, because HCOO⁻ production becomes dominant under low-intensity light, in which the Ru–Ru bond tends to form. The photochemical CO₂ reduction catalysed by [Ru(bpy)(CO)₂Cl₂]₂ (0.05 mM) shows similar time-course profiles for the production of CO and HCOO⁻ to those of *trans*(Cl)-Ru(bpy)(CO)₂Cl₂ (0.10 mM), indicating that the immediate dissociation of the dimer occurs to regenerate the monomeric complex during the CO₂ reduction. We carried out kinetic analyses based on the new reaction mechanism, and the simulation curve reproduced the concentration dependence of the product selectivity (CO/

HCOO⁻) well. In order to further verify the proposed mechanism, we synthesized *trans*(Cl)-Ru(6Mes-bpy)(CO)₂Cl₂ (Fig. 1, 6Mes-bpy: 6,6'-dimesityl-2,2'-bipyridine) which cannot form a dimer due to the bulky substituents at 6,6'-positions in 2,2'-bipyridine. The photochemical CO₂ reduction catalysed by *trans*(Cl)-Ru(6Mes-bpy)(CO)₂Cl₂ selectively produced CO, strongly supporting our proposed mechanism for formate production.

Experimental section

General procedure

[Ru(bpy)(CO)₂Cl₂]₂, [Ru(CO)₂Cl₂]_n, *trans*(Cl)-Ru(bpy)(CO)₂Cl₂, [Ru(bpy)₃](PF₆)₂, [Ru(4dmbpy)₃](PF₆)₂ (4dmbpy = 4,4'-dimethyl-2,2'-bipyridine), 6,6'-dimesityl-2,2'-bipyridine (6Mes-bpy), and BNAH were prepared according to the literature.^{73,75–78} DMA (Wako, dehydrate) was used as supplied. High-purity water (resistivity: 18.2 MΩ cm) was obtained from an ultrapure water system (RFU424TA, Advantec). Cyclic voltammograms (CVs) and differential pulse voltammograms (DPVs) were obtained using a Bio-Logic VSP Potentiostat using EC-Lab software. As the electrodes, a BAS glassy-carbon working electrode, a BAS Pt counter electrode, and a BAS RE-7 (Ag/AgNO₃ 0.01 M in acetonitrile) reference electrode were used. Absorption spectra in the spectroelectrochemical experiments were obtained on an ALS SEC2000 using an electrochemical cell of 1 mm path length incorporating the three-electrode system.

Synthesis of *trans*(Cl)-Ru(6Mes-bpy)(CO)₂Cl₂

In a 30 mL flask equipped with a reflux condenser were placed [Ru(CO)₂Cl₂]_n (30 mg), 6,6'-dimesityl-2,2'-bipyridine (6Mes-bpy; 51 mg, 0.13 mmol) and ethanol (6 mL) under an argon atmosphere, and the solution was refluxed for 18 h. As the reaction proceeded, the starting solution became a white suspension. The precipitate was filtrated and washed with ethanol. The solid was recrystallized from CHCl₃-ether to afford pale yellow crystals (45 mg, 56%): ¹H NMR (400 MHz, CDCl₃) δ 8.26 (d, *J* = 8.0 Hz, 2H), 8.09 (dd, *J* = 8.0 and 7.6 Hz, 2H), 7.45 (d, *J* = 7.6 Hz, 2H), 6.97 (s, 4H), 2.33 (s, 6H), 2.16 (s, 12H); FTIR (KBr) ν_{CO}/cm⁻¹ 1986, 2051. Anal. calcd (%) for C₃₀H₂₈Cl₂N₂O₂Ru: C, 58.07; H, 4.55; N, 4.51. Found: C, 58.11; H, 4.76; N, 4.65.

Photocatalytic CO₂ reduction

Solutions (5 mL) of the catalyst (*trans*(Cl)-Ru(bpy)(CO)₂Cl₂ or *trans*(Cl)-Ru(6Mes-bpy)(CO)₂Cl₂), [Ru(bpy)₃](PF₆)₂ and BNAH in Ar-saturated DMA/water were placed in quartz tubes (23 mL volume, i.d. = 14 mm). The solutions were bubbled through septum caps with CO₂ gas for 20 min, and then were irradiated using a 400 W high-pressure mercury lamp at λ > 400 nm (Riko Kagaku, L-39 cutoff filter) in a carousel irradiation apparatus (Riko Kagaku, RH400-10W). The reaction temperature was maintained at 298 ± 3 K by using a water bath. The gaseous products (CO and H₂) were analyzed with GC, and formate was also quantified with GC by acidifying formate to formic acid.⁴⁷

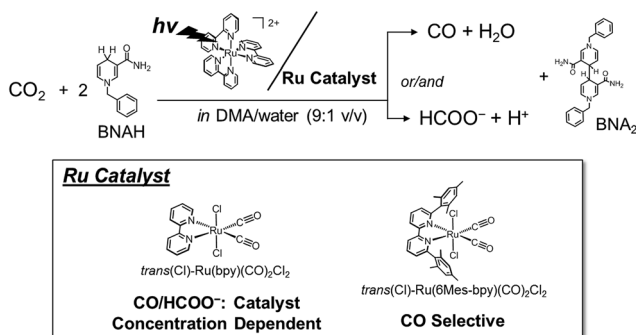


Fig. 1 Photochemical CO₂ reduction catalysed by *trans*(Cl)-Ru(bpy)(CO)₂Cl₂ or *trans*(Cl)-Ru(6Mes-bpy)(CO)₂Cl₂ in a DMA/water solution containing [Ru(bpy)₃]²⁺ and BNAH as the photosensitizer and the electron donor, respectively.



Quenching experiments

Emission from the excited state of $[\text{Ru}(\text{4dmbpy})_3](\text{PF}_6)_2$ in the Ar-saturated DMA/water solution was recorded on a Hitachi F-4500 spectrometer ($\lambda_{\text{ex}} = 453 \text{ nm}$) in the absence and in the presence of the quencher, BNAH. The Stern–Volmer relationship (eqn (1)) was obtained from the plots of the relative emission intensity (I_0/I) versus the concentration of the quencher (Q: BNAH):

$$I_0/I = 1 + K_{\text{SV}}[Q] = 1 + k_{\text{q}}\tau[Q] \quad (1)$$

where I_0 and I represent the intensity at 628 nm in the absence and the presence of the quencher, respectively, and K_{SV} , k_{q} , τ are the Stern–Volmer constant, the quenching rate constant, and the emission lifetime, respectively.

Light intensity dependence

In square quartz cells ($l = 1.0 \text{ cm}$) were placed DMA/water (9 : 1 v/v, 3 mL) solutions containing the Ru catalyst, $[\text{Ru}(\text{bpy})_3](\text{PF}_6)_2$ and BNAH, and CO_2 was bubbled through the septum caps for at least 30 min before measurement. The solutions were irradiated using a 500 W superhigh-pressure mercury lamp (Ushio, USH-500D) through a Toshiba Y-43 glass filter ($\lambda > 400 \text{ nm}$) with and without neutral-density (ND) filters. The absorption spectra of the solutions were measured with a Shimadzu MultiSpec-1500 Spectrometer. The gaseous products (CO and H_2) were analysed with GC, and formate was also quantified with GC by acidifying formate to formic acid.⁴⁷

Results and discussion

Photochemical CO_2 reduction catalysed by *trans*(Cl)–Ru(bpy)(CO)₂Cl₂

The photocatalytic CO_2 reductions were carried out in DMA/water (9 : 1 v/v) solutions containing *trans*(Cl)–Ru(bpy)(CO)₂Cl₂ (the catalyst), $[\text{Ru}(\text{bpy})_3]^{2+}$ (the photosensitizer) and BNAH (the electron donor) under visible light irradiation ($\lambda > 400 \text{ nm}$), where $[\text{Ru}(\text{bpy})_3]^{2+}$ was selectively excited and reductively quenched by BNAH to yield the reduced species of the photosensitizer, $[\text{Ru}(\text{bpy})_3]^+$.⁴⁷ The 10 vol% water content was selected for the reaction solvent because this water ratio gave the highest amount of the reduction products. The water in the reaction solution plays an important role as the transporter of the protons for the CO_2 reduction, but higher contents of water decrease the quenching efficiency of BNAH toward $[\text{Ru}(\text{bpy})_3]^{2+}$.⁴⁷ The reduction potential of *trans*(Cl)–Ru(bpy)(CO)₂Cl₂, which was estimated to be $-1.51 \text{ V vs. Ag/Ag}^+$ in DMA/water (9 : 1 v/v) with the use of the differential pulse voltammetry (Fig. S1 in ESI[†]), indicates that electron transfer can occur thermodynamically from the reduced photosensitizer ($[\text{Ru}(\text{bpy})_3]^{2+/+}$: $-1.68 \text{ V vs. Ag/Ag}^+$)⁴⁷ to *trans*(Cl)–Ru(bpy)(CO)₂Cl₂.

Fig. 2 shows the time-courses of the products in the photochemical CO_2 reduction in the CO_2 -saturated DMA/water (9 : 1 v/v) solution containing *trans*(Cl)–Ru(bpy)(CO)₂Cl₂ ((a) 0.10 mM and (b) 5.0 μM), $[\text{Ru}(\text{bpy})_3]^{2+}$ (0.50 mM) and BNAH (0.10 M). The

profiles show that CO and formate are selectively yielded, with scarce accompanying H_2 evolution even in the aqueous solutions, suggesting that the reduced catalyst reacts much more favourably with CO_2 than H^+ . The turnover number (TON) for the total amount of CO and formate was *ca.* 300 at 0.10 mM of the catalyst after photo-irradiation for 4 h. When 5.0 μM of *trans*(Cl)–Ru(bpy)(CO)₂Cl₂ was used, the TON was dramatically improved to *ca.* 4000, because there was no superfluous catalyst at the lower concentration. However, the rate of the formation of the products becomes slow over 2 hours. In our previous work, we reported that these effects are mainly attributable to the decrease of BNAH and the increase of BNA_2 .⁴⁷ The latter depresses the photochemical CO_2 reduction because BNA_2 reductively quenches the excited state of $[\text{Ru}(\text{bpy})_3]^{2+}$ faster than BNAH, but the back electron transfer is much more efficient.

It is worth noting that the product ratio of CO/HCOO^- in Fig. 2 is notably higher at 5.0 μM of *trans*(Cl)–Ru(bpy)(CO)₂Cl₂ than that at 0.1 mM. For example, the ratio of CO/HCOO^- is approximately 2 at 0.1 mM of the catalyst but *ca.* 7 at 5.0 μM after 30 min of photo-irradiation. Fig. 3 shows the dependence of the amounts of CO and formate and the product ratio of CO/HCOO^- on the catalyst concentration after 30 min of photo-irradiation, which reflects the initial reaction rates of the CO_2 reduction. In Fig. 3 (bottom), the initially increased product ratio of CO/HCOO^- is lowered by increasing the catalyst concentration. The unexpected profile of the product ratio comes from the differing behaviours of the initial production rates of CO and formate: the rate of CO formation increases as the catalyst concentration increases up to 20–30 μM , then decreases as the concentration increases above 30 μM , while the rate of formate production continues to increase as the catalyst concentration increases. In Fig. 3 (bottom), the increase in the product ratio with increasing catalyst concentration from 0 to 5.0 μM comes from the contribution of the blank products, which are detected even in the absence of *trans*(Cl)–Ru(bpy)(CO)₂Cl₂. It is known that $[\text{Ru}(\text{bpy})_3]^{2+}$ releases the bipyridyl ligand by photo-labilization to provide catalytically active species, resulting in the blank products.^{57,70} The amounts of the blank products are 11 and 4 μmol for CO and formate, respectively, and the blank product ratio of CO/HCOO^- is *ca.* 3. Thus, if the blank products caused by $[\text{Ru}(\text{bpy})_3]^{2+}$ were excluded, the selectivity of CO would continue to increase with decreasing catalyst concentration.

Changes in the electronic absorption spectra during the photo-irradiation and light intensity dependence of the product selectivity

As shown in Fig. 3, the product selectivity of CO/HCOO^- was affected by the catalyst concentration. The behaviour led us to consider that an association of the catalyst occurs during the CO_2 reduction. The photo-irradiation of an Ar-saturated DMA/water solution containing *trans*(Cl)–Ru(bpy)(CO)₂Cl₂ (0.20 mM), $[\text{Ru}(\text{bpy})_3]^{2+}$ and BNAH produced H_2 instead of CO and formate. During the photo-irradiation, the solution colour changed from orange to dark red. The spectra of the Ar-saturated reaction solution showed the appearance of a characteristic broad peak



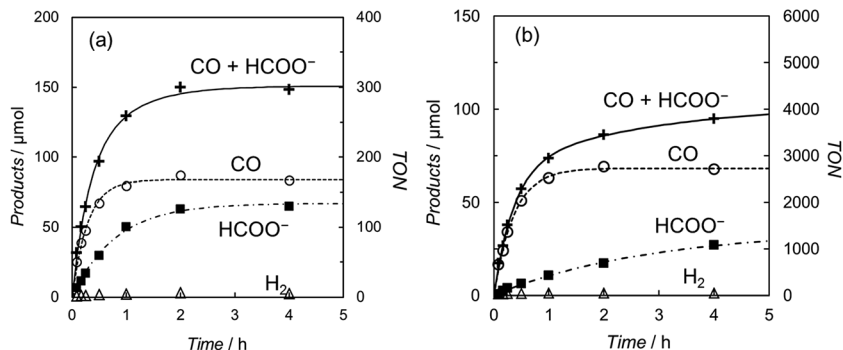


Fig. 2 Photo-irradiation time dependence of the products in a CO₂-saturated DMA/water (9 : 1 v/v) solution containing (a) 0.1 mM and (b) 5.0 μM of *trans*(Cl)-Ru(bpy)(CO)₂Cl₂, [Ru(bpy)₃](PF₆)₂ (0.50 mM) and BNAH (0.10 M): CO (○), HCOO⁻ (■), H₂ (Δ) and CO + HCOO⁻ (+).

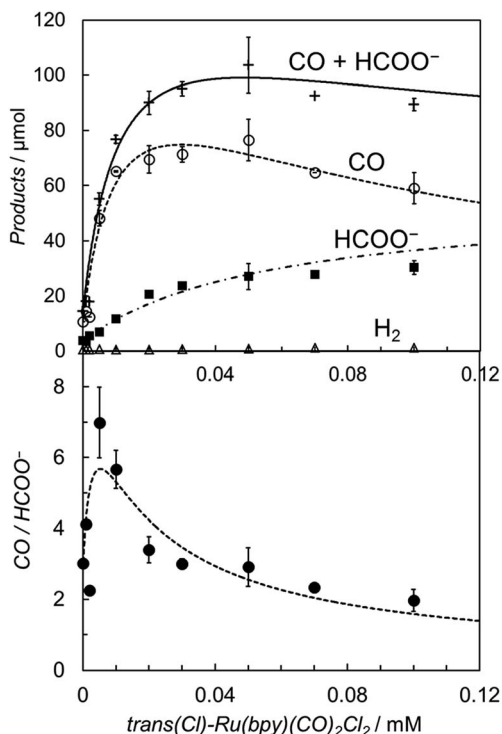


Fig. 3 (Top) Plots of the amounts of the reduction products after 30 min of photo-irradiation (400 W Hg lamp, $\lambda > 400$ nm) versus the concentration of *trans*(Cl)-Ru(bpy)(CO)₂Cl₂ in CO₂-saturated DMA/water (9 : 1 v/v) in the presence of [Ru(bpy)₃](PF₆)₂ (0.50 mM) and BNAH (0.10 M): CO (○), HCOO⁻ (■), H₂ (Δ) and CO + HCOO⁻ (+). (Bottom) Plots of the CO/HCOO⁻ ratio versus the concentration of *trans*(Cl)-Ru(bpy)(CO)₂Cl₂. The curves represent the theoretical fittings based on the kinetic analyses (see eqn (3) and (5)).

at 700–800 nm (Fig. 4a), indicating that the polymeric ruthenium complex, [Ru(bpy)(CO)₂]_n, formed by the reduction of *trans*(Cl)-Ru(bpy)(CO)₂Cl₂.^{49,79,80} On the other hand, photo-irradiation (400 W high-pressure mercury lamp without the ND filter, $\lambda > 400$ nm) under a CO₂ atmosphere showed no colour change of the solution, suggesting that the reduced catalyst was oxidized by coordination with CO₂ to suppress the formation of the polymeric complex. It has been reported that *trans*(Cl)-Ru(bpy)(CO)₂Cl₂ is electrochemically reduced to form the

polymeric ruthenium complex *via* the Ru(I)–Ru(I) dimer (Scheme 2).^{71,72} As the absorption band of the dimer overlaps with that of [Ru(bpy)₃]²⁺ (Fig. 4b), the formation of the dimer could not be observed using the absorption spectra. Thus, if the product selectivity of CO/HCOO⁻ is related to an association of the catalysts, and changes to the absorption spectrum of the reaction solution are not observed during the photo-irradiation, the associated species might be the ruthenium dimeric complex.

Fig. 4c and d show the spectra during photochemical CO₂ reduction under high- and low-intensity light (500 W superhigh-pressure mercury lamp without and with the ND filters, $\lambda >$

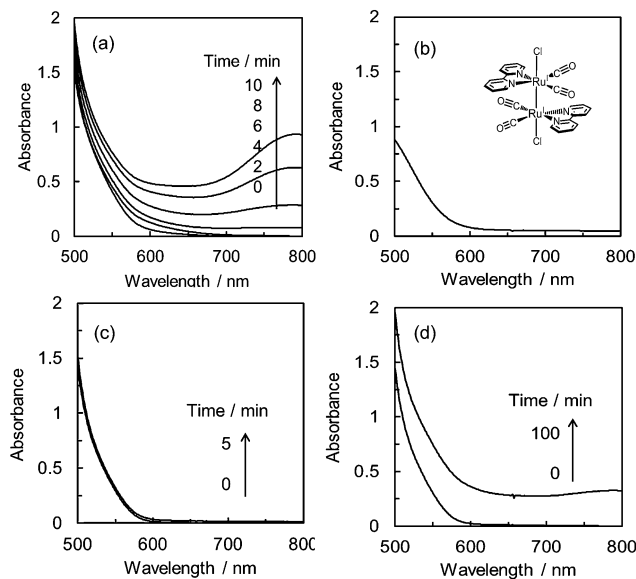


Fig. 4 (a) Absorption spectra of an Ar-saturated DMA/water (9 : 1 v/v) solution containing *trans*(Cl)-Ru(bpy)(CO)₂Cl₂ (0.20 mM), [Ru(bpy)₃](PF₆)₂ (0.50 mM) and BNAH (0.10 M) during photo-irradiation with $\lambda > 400$ nm light with an intensity of 7.5×10^{-7} einstein s⁻¹. (b) Absorption spectrum of [Ru(bpy)(CO)₂Cl₂] (0.40 mM) in DMA/water (9 : 1 v/v). (c) Absorption spectra of CO₂-saturated DMA/water (9 : 1 v/v) solutions containing *trans*(Cl)-Ru(bpy)(CO)₂Cl₂ (0.10 mM), [Ru(bpy)₃](PF₆)₂ (0.50 mM) and BNAH (0.10 M) by photo-irradiation with $\lambda > 400$ nm light of 7.5×10^{-7} einstein s⁻¹ and (d) 3.8×10^{-8} einstein s⁻¹ (total incident light: 2.3×10^{-4} einstein).

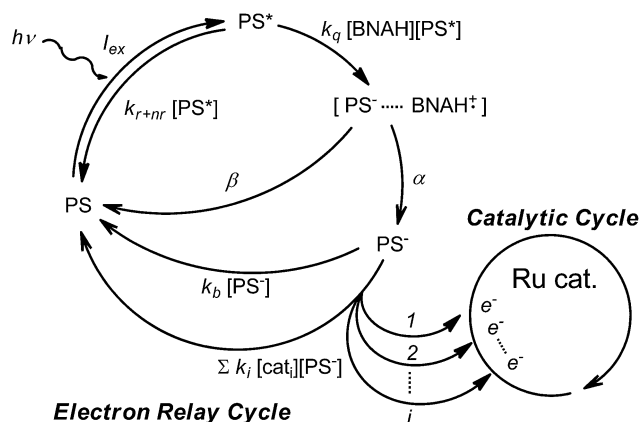


400 nm). The irradiation time was adjusted for the total incident light to be 2.3×10^{-4} einstein. While no spectral change is observed in Fig. 4c, a polymeric absorption at 700–800 nm appears in Fig. 4d. This indicates that the Ru–Ru bond tends to form under the lower-intensity light.

We have further investigated the light intensity dependence of the product selectivity in the photochemical CO₂ reduction. Fig. 5 shows the light intensity dependence of the product ratio at a dilute concentration of *trans*(Cl)–Ru(bpy)(CO)₂Cl₂ (20 μM). The ratio of CO/HCOO[−] decreases with reduction of the light intensity, that is, the formation of HCOO[−] becomes dominant at lower light intensity. Since the concentration of 20 μM was selected to prevent the formation of the polymer that caused a dramatic decrease of the effective catalyst concentration in the solution, we could exclude the possibility that the polymeric species contributed to the product selectivity. Considering that the low-intensity light induces the Ru–Ru bond formation, the most plausible key intermediate for forming HCOO[−] would be the ruthenium dimer.

Mechanistic insight into product selectivity

The photochemical CO₂ reduction system consists of two parts: an electron relay cycle and a catalytic cycle (Scheme 3). In the electron relay cycle, the excited state of the photosensitizer (PS*) and BNAH form the encounter complex, where electron transfer from BNAH to PS* occurs to produce the charge-separated state ([PS[−]...BNAH⁺]).^{81,82} Dissociation of the encounter complex gives the free reduced photosensitizer (PS[−]), which could supply electrons to the catalyst. In Scheme 3, I_{ex} is the rate of incident photons, k_q is the quenching rate constant by BNAH, k_{r+nr} is the sum of the radiative and non-radiative rate constants of the PS*, α is the cage escape efficiency after the electron transfer from BNAH to the PS*,⁸² β is the fraction of back-electron transfer in the solvent cage ($\beta = 1 - \alpha$), k_b is the quenching rate constant of the PS[−], k_i is the electron transfer rate constant from the PS[−] to the *i*th form of the catalyst, and [cat_{*i*}] is the concentration of the *i*th form of the catalyst. In the initial stage of the reaction, the



Scheme 3 The electron relay cycle and the catalytic cycle in the photochemical CO₂ reduction.

quenching by BNA₂ can be ignored.⁴⁷ The steady-state concentration of the PS[−] is evaluated as a function of the concentration of the catalyst (eqn (2)) by applying the steady state approximation to Scheme 3:

$$[\text{PS}^-] = \frac{(\alpha k_q [\text{BNAH}] I_{\text{ex}}) / \{k_b (k_{r+nr} + k_q [\text{BNAH}])\}}{1 + \sum_i k_i [\text{cat}_i] / k_b} \quad (2)$$

According to eqn (2), when the light intensity and the concentration of BNAH are constant, the steady-state concentration of the PS[−] is affected by the catalyst concentration: [PS[−]] decreases as the catalyst concentration increases.

In the catalytic cycle, we have assumed that the dimeric complex produces formate while the monomeric complex produces CO through reaction with CO₂ (Scheme 4). It has been reported that the one-electron-reduced catalyst (Ru⁺) does not react with CO₂ (ref. 48–56, 69, 70 and 83) but instead forms a dimer Ru⁺–Ru⁺.^{71,72} Therefore the resting state in the catalytic cycle would be the Ru⁺ species. In the low concentration region of the catalyst, it is possible for the catalyst to accept two electrons smoothly from the PS[−]. On the other hand, in the high concentration region, the amount of the PS[−] would not be enough for the catalyst to receive two electrons smoothly. In particular, in the photochemical reaction, electron transfer to the catalyst hardly occurs, and accordingly the Ru⁺ remains unreacted.

The valence of the ruthenium centre in the dimer is possibly changed by the reaction with CO₂ and H⁺. When the Ru(II) valence state forms, the Ru–Ru bond would dissociate into the monomeric species. In order to confirm the cleavage of the Ru–Ru bond, we examined the photocatalytic CO₂ reduction by [Ru(bpy)(CO)₂Cl]₂, which was separately prepared.⁷³ According to the reduction potential of [Ru(bpy)(CO)₂Cl]₂, which is estimated to be ca. −1.6 V vs. Ag/Ag⁺ in DMA/water (9 : 1 v/v) (Fig. S2 in ESI[†]), electron transfer can thermodynamically occur from the reduced photosensitizer to the dimer. The reaction catalysed by 0.05 mM of [Ru(bpy)(CO)₂Cl]₂ (0.10 mM of the Ru unit) showed very similar time–course profiles of CO and HCOO[−] to

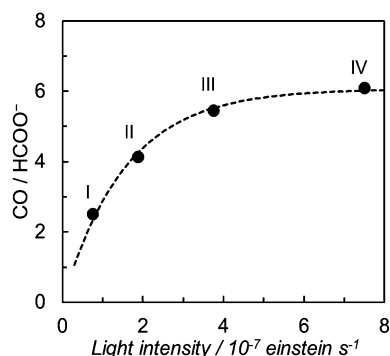
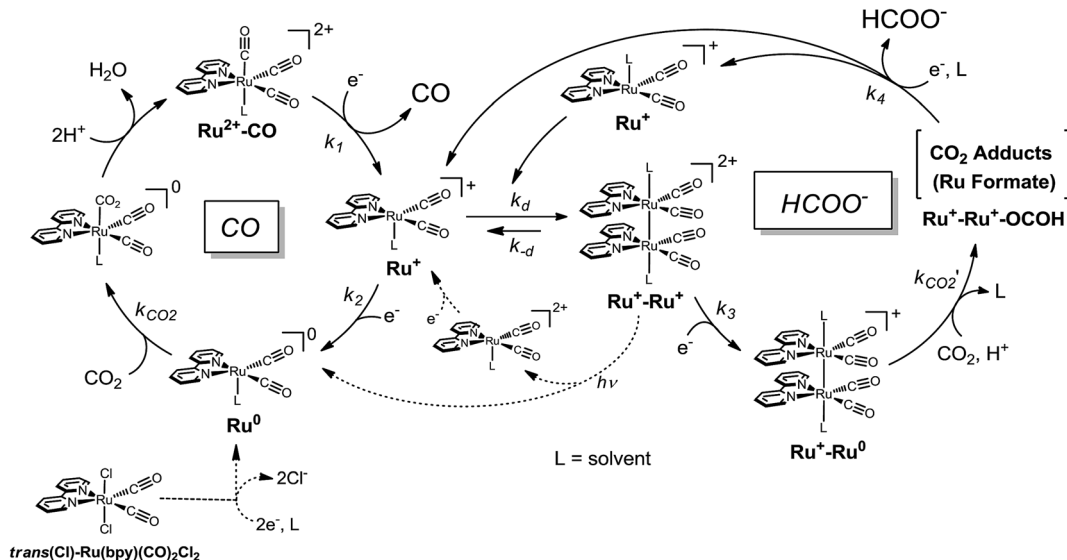


Fig. 5 Light intensity dependence of the product ratio of CO/HCOO[−] in DMA/water (9 : 1 v/v) solutions containing *trans*(Cl)–Ru(bpy)(CO)₂–Cl₂ (20 μM), [Ru(bpy)₃](PF₆)₂ (0.50 mM) and BNAH (0.10 M) during photo-irradiation with λ > 400 nm light. The photo-irradiation times were (I) 50 min, (II) 20 min, (III) 10 min and (IV) 5 min (total incident light: 2.3×10^{-4} einstein).



Scheme 4 Plausible mechanism for CO₂ reduction.

those of 0.10 mM of *trans*(Cl)-Ru(bpy)(CO)₂Cl₂ (Fig. S3 in ESI[†]). This result supports formate production being accompanied with the cleavage of the Ru–Ru bond to regenerate the monomeric species. We carried out the photo-irradiation of a concentrated solution of [Ru(bpy)(CO)₂Cl]₂ (0.40 mM) in Ar-saturated DMA/water without either the photosensitizer or the electron donor. The direct photo-irradiation of the dimer results in the appearance of a broad absorption corresponding to the polymeric species, suggesting that disproportionation of the Ru(I)–Ru(I) dimer occurs (Scheme 4). The disproportionation of the dimer has been proposed in the isomerization from *trans*(Cl) to *cis*(Cl)-Ru(bpy)(CO)₂Cl₂, which is induced by the addition of NaBH₄.⁸⁴ However, in the reaction conditions in the presence of [Ru(bpy)₃]²⁺ (0.50 mM) as the photosensitizer, direct photo-excitation of the dimer scarcely occurs because most of the light is absorbed by the photosensitizer when the concentration of the dimer is low. In addition, we have observed that [Ru(bpy)(CO)₂Cl]₂ is stable against CO₂ in DMA/water in the dark. Thus, it is thought that formate production would start with the electrical reduction of Ru⁺–Ru⁺.

The relationship between the concentration of the catalyst and the initial rates for the formation of CO and formate was evaluated by applying the steady state approximation to Scheme 4 and using eqn (2). The equations for CO and formate are expressed as the following eqn (3) and (4), respectively (See ESI[†]):

$$v_{\text{CO}} = v_0 + \frac{a[\text{cat}]_i}{b[\text{cat}]_i^2 + c[\text{cat}]_i + d} \quad (3)$$

$$v_{\text{HCOO}^-} = v'_0 + \frac{a'[\text{cat}]_i^2}{b'[\text{cat}]_i^2 + c'[\text{cat}]_i + d'} \quad (4)$$

where v_{CO} and v_{HCOO^-} are the formation rates of CO and formate, which can be calculated by dividing the concentration in mol of the products after photo-irradiation for 30 min by the

volume of the reaction solution (5.0 mL) and the time (1800 s); [cat]_i is the initial concentration of *trans*(Cl)-Ru(bpy)(CO)₂Cl₂; γ is a proportional constant particular to the catalyst, $\gamma = [\text{Ru}^+]/[\text{cat}]_i$; v_0 and v'_0 are the blank formation rates caused by [Ru(bpy)₃]²⁺; a, b, c, d, a', b', c' and d' are the constant values as expressed by the following: $a = (k_2 k_{-d} \alpha k_q [\text{BNAH}] I_{\text{ex}} \gamma) / (k_{n+nr} + k_q [\text{BNAH}])$, $b = b' = 2 k_d k_3 \gamma^2$, $c = c' = 2 k_{-d} k_2 \gamma$, $d = k_b k_{-d} + (k_3 \alpha k_q [\text{BNAH}] I_{\text{ex}}) / (k_{n+nr} + k_q [\text{BNAH}])$, $a' = (k_3 k_d \alpha k_q [\text{BNAH}] I_{\text{ex}} \gamma^2) / (k_{n+nr} + k_q [\text{BNAH}])$, $d' = k_b k_{-d}$. The value of γ is related to k_{CO_2} and k_{CO_2}' , and a higher value of γ would indicate a higher reaction rate of the two-electron-reduced catalyst with CO₂ and H⁺.

In Fig. 3 top, curve fitting according to eqn (3) gives the parameters: $v_0 = 1.2 \times 10^{-6} \text{ M s}^{-1}$, $a/d = 1.1 \text{ s}^{-1}$, $b/d = 1.1 \times 10^9 \text{ M}^{-2}$, $c/d = 9.1 \times 10^4 \text{ M}^{-1}$. The simulation curve well reproduces the experimental behaviour, where the rate increases as the catalyst concentration increases up to 20–30 μM then decreases as the concentration increases above 30 μM . Eqn (4) can be simplified when the d' term is negligible (Fig. S9 in ESI[†]):

$$v_{\text{HCOO}^-} = v'_0 + \frac{a'[\text{cat}]_i}{b'[\text{cat}]_i + c'} \quad (5)$$

By assuming $v'_0 = 4.2 \times 10^{-7} \text{ M s}^{-1}$, the double-reciprocal plots of the rate of formate production versus the concentration of *trans*(Cl)-Ru(bpy)(CO)₂Cl₂ give $a'/c' = 0.10 \text{ s}^{-1}$ and $b'/c' = 1.8 \times 10^4 \text{ M}^{-1}$ (Fig. 6). These simulation curves based on eqn (3) and (5) agree well with the experimental plots in Fig. 3 (top), and also reproduce the results for the selectivity in Fig. 3 (bottom).

In eqn (3)–(5), the following relationships should be satisfied; $b/c = b'/c'$ and $a/c = a'/b'$. From eqn (3) and (5), b/c and b'/c' are estimated to be $1.3 \times 10^4 \text{ M}^{-1}$ and $1.8 \times 10^4 \text{ M}^{-1}$, and a/c and a'/b' to be $1.2 \times 10^{-5} \text{ M s}^{-1}$ and $0.6 \times 10^{-5} \text{ M s}^{-1}$, respectively. The results of the curve fittings satisfy the theoretical requirements. Furthermore, a/c and a'/b' are expressed as eqn



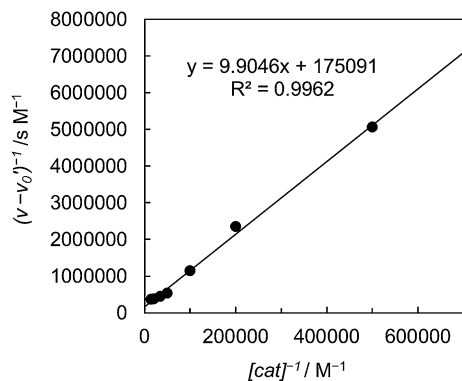


Fig. 6 Double-reciprocal plots of the rate of the formate production versus the concentration of *trans*(Cl)-Ru(bpy)(CO)₂Cl₂.

(6) and the value can be estimated using the values $k_q = 2.6 \times 10^8 \text{ M}^{-1} \text{ s}^{-1}$, $k_{r+nr} = 1.2 \times 10^6 \text{ s}^{-1}$ and $\alpha I_{\text{ex}} = 3.3 \times 10^{-5} \text{ M s}^{-1}$, which are obtained from the Stern–Volmer plot, the emission lifetime of the excited [Ru(bpy)₃]²⁺ and the simulation curve of the decrease of BNAH, respectively.⁴⁷

$$\frac{\alpha k_q [\text{BNAH}] I_{\text{ex}}}{2(k_{r+nr} + k_q [\text{BNAH}])} = 1.6 \times 10^{-5} \text{ M s}^{-1} \quad (6)$$

This value is consistent with those of *a/c* and *a'/b'* estimated from eqn (3) and (5), indicating that the kinetic analyses strongly support the proposed mechanism.

Photochemical CO₂ reduction using [Ru(4dmbpy)₃]²⁺ as photosensitizer

As the photosensitizer in the photochemical CO₂ reduction, we used [Ru(bpy)₃]²⁺, whose first reduction potential is $-1.68 \text{ V vs. Ag/Ag}^+$ in DMA/water (9 : 1 v/v).⁴⁷ In order to investigate the effect of the photosensitizer on the product selectivity, we used [Ru(4dmbpy)₃]²⁺ (4dmbpy = 4,4'-dimethyl-2,2'-bipyridine) instead of [Ru(bpy)₃]²⁺. [Ru(4dmbpy)₃]²⁺ has a more negative reduction potential of $-1.77 \text{ V vs. Ag/Ag}^+$ (Fig. S4†) than that of [Ru(bpy)₃]²⁺, indicating that [Ru(4dmbpy)₃]²⁺ works as a powerful reductant after the photo-induced electron transfer from BNAH is completed. However, the more negative potential of [Ru(4dmbpy)₃]²⁺ makes the quenching rate constant by BNAH more inefficient ($k_q \sim 1.7 \times 10^7 \text{ M}^{-1} \text{ s}^{-1}$)⁸⁵ than that of [Ru(bpy)₃]²⁺ ($k_q = 2.6 \times 10^8 \text{ M}^{-1} \text{ s}^{-1}$)⁴⁷ by one order of magnitude or more.

Fig. 7 shows the relationship between the concentration of the catalyst and the initial rates for CO and formate production using [Ru(4dmbpy)₃]²⁺. The simulation curves based on eqn (3) and (4) well reproduce the experimental plots, where formate shows an induction region for its production at very low concentration, and the plots for CO show a downward convex shape at high concentration. From the curve fittings in Fig. 7 and the blank experiment involving [Ru(4dmbpy)₃]²⁺ the parameters are given as: $v_0 = 1.5 \times 10^{-6} \text{ M s}^{-1}$, $a/d = 2.5 \text{ s}^{-1}$, $b/d = 1.0 \times 10^{10} \text{ M}^{-2}$, $c/d = 7.7 \times 10^5 \text{ M}^{-1}$, $v_0' = 2.2 \times 10^{-7} \text{ M s}^{-1}$, $a'/d' = 1.5 \times 10^4 \text{ M}^{-1} \text{ s}^{-1}$, $b'/d' = 8.4 \times 10^9 \text{ M}^{-2}$, $c'/d' = 2.1 \times 10^5$

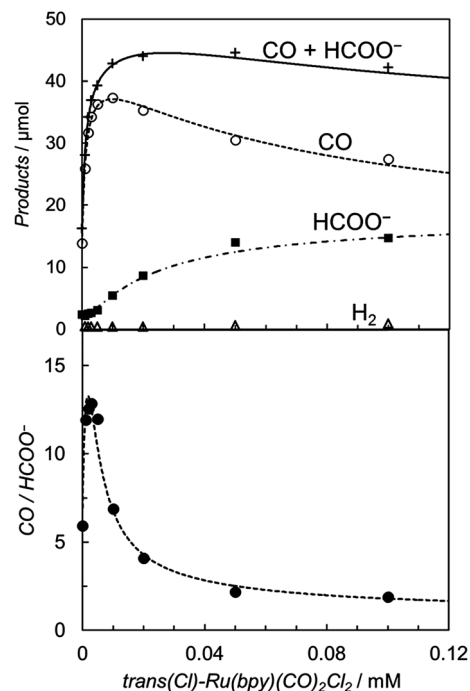


Fig. 7 (Top) Plots of the amounts of the reduction products after 30 min of photo-irradiation (400 W Hg lamp, $\lambda > 400 \text{ nm}$) versus the concentration of *trans*(Cl)-Ru(bpy)(CO)₂Cl₂ in CO₂-saturated DMA/water (9 : 1, v/v) in the presence of [Ru(4dmbpy)₃](PF₆)₂ (0.50 mM) and BNAH (0.10 M): CO (○), HCOO⁻ (■), H₂ (Δ) and CO + HCOO⁻ (+). (Bottom) Plots of the CO/HCOO⁻ ratio versus the concentration of *trans*(Cl)-Ru(bpy)(CO)₂Cl₂. The curves represent the theoretical fittings based on the kinetic analyses (see eqn (3) and (4)).

M^{-1} . While the values of *b/c* and *b'/c'*, estimated to be $1.3 \times 10^4 \text{ M}^{-1}$ and $4.0 \times 10^4 \text{ M}^{-1}$, are similar to those using [Ru(bpy)₃]²⁺ (*b/c* = $1.3 \times 10^4 \text{ M}^{-1}$ and *b'/c'* = $1.8 \times 10^4 \text{ M}^{-1}$ in Fig. 3), the values of *a/c* and *a'/b'*, estimated to be $3.3 \times 10^{-6} \text{ M s}^{-1}$ and $1.8 \times 10^{-6} \text{ M s}^{-1}$, are smaller than those using [Ru(bpy)₃]²⁺ (*a/c* = $1.2 \times 10^{-5} \text{ M s}^{-1}$ and *a'/b'* = $0.6 \times 10^{-5} \text{ M s}^{-1}$ in Fig. 3). Assuming that the cage escape efficiency is the same as that for [Ru(bpy)₃]²⁺ ($\alpha I_{\text{ex}} = 3.3 \times 10^{-5} \text{ M s}^{-1}$), the value of eqn (6) is estimated to be $9.4 \times 10^{-6} \text{ M s}^{-1}$ using the quenching rate constant of [Ru(4dmbpy)₃]²⁺. Thus, the smaller values of *a/c* and *a'/b'* estimated in Fig. 7 well reflect the smaller quenching rate constant (k_q) of [Ru(4dmbpy)₃]²⁺. In addition, the maximum selectivity attained for the products ratio is *ca.* 13 at the concentration of 3 μM of the catalyst, indicating that the selectivity of CO is higher than that observed in Fig. 3. The result implies that the reduction potential of Ru⁺ is more negative than that of Ru²⁺-CO in Scheme 4, and that the powerful reductant smoothly supplies the second electron to Ru⁺ in the low catalyst concentration region.

Selective CO formation in photochemical CO₂ reduction using *trans*(Cl)-Ru(6Mes-bpy)(CO)₂Cl₂

While we have succeeded in explaining the product selectivity with the kinetic analyses, we have not yet directly detected the dimer during the CO₂ reduction reaction by means of



spectroscopic methods such as UV-vis absorption and ESI-MS. This is because the absorption band of the dimer is overlapped with that of $[\text{Ru}(\text{bpy})_3]^{2+}$ and the absorption coefficient of the dimer at 450 nm is around one-quarter smaller than that of $[\text{Ru}(\text{bpy})_3]^{2+}$ (Fig. 4b).⁸⁶ Even if all of the *trans*(Cl)-Ru(bpy)(CO)₂Cl₂ (0.1 mM) transforms into the Ru(I)-Ru(I) dimer during the photochemical reaction, the contribution of the dimer would be only 2.5% of the whole absorption. In addition, polymerization easily occurs even in CO₂-saturated DMA/water when a high concentration (>0.2 mM) of *trans*(Cl)-Ru(bpy)(CO)₂Cl₂ is used. The attempt to detect the intermediate by ESI-MS has also failed so far due to the lower stability during the ionization process of the measurement. Thus, we changed the strategy to verify the proposed mechanism: we synthesized a novel ruthenium complex, *trans*(Cl)-Ru(6Mes-bpy)(CO)₂Cl₂, which has mesityl groups at the 6,6'-positions of the bipyridine ligand to suppress dimer formation, and investigated the product selectivity in the photocatalytic CO₂ reduction.

The synthesis is described in the experimental section. The reduction potential of *trans*(Cl)-Ru(6Mes-bpy)(CO)₂Cl₂ (-1.56 V vs. Ag/Ag⁺ in DMA/water (9 : 1 v/v), Fig. S7 in ESI[†]) is similar to that of *trans*(Cl)-Ru(bpy)(CO)₂Cl₂, indicating that the mesityl groups do not strongly affect the electronic structure. This also suggests that the electron transfer reaction from the reduced photosensitizer to *trans*(Cl)-Ru(6Mes-bpy)(CO)₂Cl₂ occurs similarly to that of *trans*(Cl)-Ru(bpy)(CO)₂Cl₂. Before performing the photocatalytic CO₂ reduction, we checked that *trans*(Cl)-Ru(6Mes-bpy)(CO)₂Cl₂ does not form a dimer by monitoring the absorption spectra of the solutions containing the ruthenium complex, $[\text{Ru}(\text{bpy})_3]^{2+}$ and BNAH during photo-irradiation under an Ar atmosphere. In contrast to *trans*(Cl)-Ru(bpy)(CO)₂Cl₂, as shown in Fig. 4a, no absorption band corresponding to the polymeric complex is observed, as shown in Fig. 8, indicating that the bulky substituents at the 6,6'-positions of the bipyridyl ligand suppress the formation of the Ru-

Ru bond. The differential absorption spectra show small changes to the spectra with a broad shoulder between 550 and 600 nm (see the inset in Fig. 8). They are comparable with the changes to the spectra in electrolysis (Fig. S8 in the ESI[†]), because in the spectra measured during the photo-reaction (Fig. 8), the absorptions of the photosensitizer and the electron donor overlap. The changes in the spectra during the photo-reaction would be due to formation of the one-electron reduced but non-dimerised species of the ruthenium complex.

The photocatalytic CO₂ reduction was carried out using *trans*(Cl)-Ru(6Mes-bpy)(CO)₂Cl₂ as the catalyst in a DMA/water (9 : 1 v/v) solution containing $[\text{Ru}(\text{bpy})_3]^{2+}$ (0.50 mM) as the photosensitizer and BNAH (0.10 M) as the electron donor. The relationships between the concentration of the catalyst and the amounts of CO and formate are shown in Fig. 9. In contrast with Fig. 3, Fig. 9 shows that CO mainly forms, accompanied by a small amount of formate. The formate production is independent of the catalyst concentration, indicating that the formate comes from the blank reaction by $[\text{Ru}(\text{bpy})_3]^{2+}$. The plots of the CO production versus the catalyst concentration are well fitted by the kinetic analysis based on the mechanism which does not include dimer formation. When the dimer formation is negligible in Scheme 3 and 4, the production rate for CO is expressed as eqn (7) (ESI[†]):

$$v_{\text{CO}} = v_0 + \frac{a''[\text{cat}]_t}{b''[\text{cat}]_t + c''} \quad (7)$$

where a'' , b'' and c'' are the constant values as expressed by the following: $a'' = k_2 \alpha k_q [\text{BNAH}] I_{\text{ex}} \gamma$, $b'' = 2 k_2 (k_{n+nr} + k_q [\text{BNAH}]) \gamma$, $c'' = k_b (k_{n+nr} + k_q [\text{BNAH}])$. Curve fitting based on eqn (6) gives the parameters: $v_0 = 2.4 \times 10^{-6} \text{ M s}^{-1}$, $a''/b'' = 0.85 \times 10^{-5} \text{ M s}^{-1}$, $c''/b'' = 2.7 \times 10^{-5} \text{ M}$. The value of a''/b'' is also consistent with the value ($1.6 \times 10^{-5} \text{ M s}^{-1}$) in eqn (6). Thus, *trans*(Cl)-Ru(6Mes-bpy)(CO)₂Cl₂, which does not form a dimer, affords CO selectively in the photocatalytic CO₂ reduction.⁸⁷

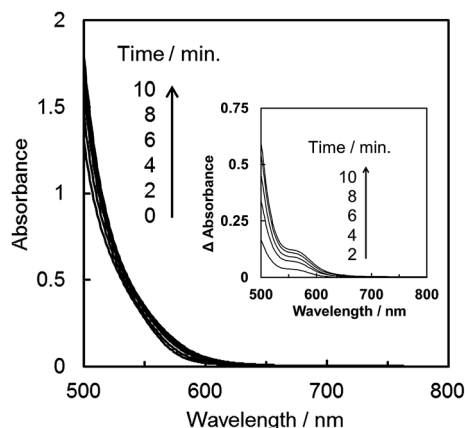


Fig. 8 Absorption spectra of the DMA/water (9 : 1, v/v) solution containing *trans*(Cl)-Ru(6Mes-bpy)(CO)₂Cl₂ (0.20 mM), $[\text{Ru}(\text{bpy})_3]^{2+}$ (0.50 mM) and BNAH (0.10 M) during the photo-irradiation with $\lambda > 400 \text{ nm}$ light with an intensity of $7.5 \times 10^{-7} \text{ einstein s}^{-1}$ under an Ar atmosphere. The inset shows the differential absorption spectra (optical path length: 10 mm).

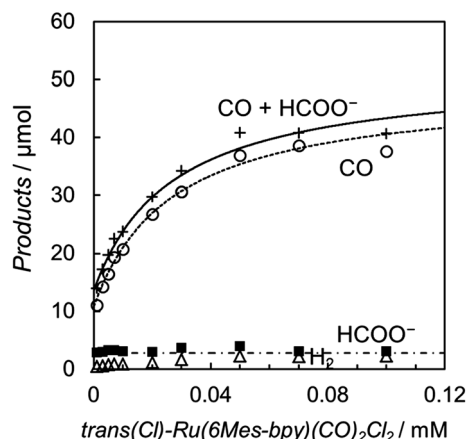


Fig. 9 Plots of the amounts of the reduction products after 15 min of photo-irradiation (400 W Hg lamp, $\lambda > 400 \text{ nm}$) versus the concentration of *trans*(Cl)-Ru(6Mes-bpy)(CO)₂Cl₂ in CO₂-saturated DMA/water (9 : 1, v/v) in the presence of $[\text{Ru}(\text{bpy})_3]^{2+}(\text{PF}_6)_2$ (0.50 mM) and BNAH (0.10 M): CO (○), HCOO⁻ (■), H₂ (△) and CO + HCOO⁻ (+). The curve for CO represents the theoretical fittings based on the kinetic analysis (see eqn (7)).



Deronzier and Zissel *et al.* reported that electrochemical CO₂ reduction using ruthenium polymers such as [Ru(bpy)(CO)₂]_n affords CO selectively.^{63–68} These reports seem to be inconsistent with our results. It should be noted that the electrochemical reactions are different from the photochemical catalyses. In the electrochemical reaction, electrons can be efficiently supplied from the electrodes to the catalysts, resulting in the valences of the most ruthenium complexes being reduced to 0 or lower, to –1.⁶⁸ On the contrary, in the photochemical catalyses discussed in this report, reduction of the catalysts occurs *via* the reaction between the reduced species of the photosensitizer and the catalyst. In the catalyses, there are various possible intermediates and reaction paths. The major reaction pathway is strongly dependent on the reaction (*e.g.*, photochemical or electrochemical reaction) and the conditions (*e.g.*, solvents, pH). The experimental results in this report suggest that the Ru(II) species of the dimer plays an important role in the reaction mechanism of formate production. It still remains unknown how the Ru(II) dimer can selectively produce formate from CO₂. Further computational studies of the process are now under way.

Conclusion

We have carried out photochemical CO₂ reduction catalyzed by *trans*(Cl)–Ru(bpy)(CO)₂Cl₂, and have unexpectedly found that the product ratio of CO to formate depends on the concentration of the catalyst. In order to explain the behavior of the CO/HCOO[–] selectivity, we have proposed a new reaction mechanism containing the formation of a catalyst dimer which selectively produces formate. The mechanism has strongly been supported by the kinetic analyses, the catalyses by [Ru(bpy)(CO)₂Cl]₂ and the light intensity dependence of the CO/HCOO[–] selectivity. The mechanism of the photocatalytic CO₂ reduction consists of the electron relay cycle and the catalytic CO₂ reduction cycle. The former is the process in which the reduced photosensitizer (PS[–]) supplies electrons to the catalyst, and the latter is the steps where the ruthenium complexes catalytically reduce CO₂ by using the supplied electrons. At high catalyst concentration, the electron relay system would be rate-determining because the catalysis becomes faster than the electron supply. Under this condition, the ruthenium catalyst cannot be supplied with sufficient electrons; the one-electron reduced species of the catalyst is not able to receive more electrons, and it forms the dimer, which produces HCOO[–]. Therefore as the catalyst concentration increases, the product selectivity (CO/HCOO[–]) decreases. As the light intensity is reduced, the concentration of PS[–] also decreases, resulting in the same effect as a high concentration of the catalyst. The mechanism also explains the photo-irradiation time dependence of the CO₂ reduction: the CO production reaches saturation. At longer reaction times, the electron donor BNAH is consumed to decrease the concentration of PS[–]. In this situation, the one-electron reduced species of the catalyst is not able to receive more electrons and forms the catalyst dimer, making the CO production decrease. However, the HCOO[–] formation continues until the electron donor is exhausted. We have

further designed and synthesized a novel ruthenium complex, *trans*(Cl)–Ru(6Mes-bpy)(CO)₂Cl₂, which has a bulky ligand to eliminate the contribution of the dimer. By suppressing the dimer formation, the photochemical CO₂ reduction produces CO selectively. Among photocatalytic systems for the CO₂ reduction by ruthenium complexes, to the best of our knowledge, this system is the first case producing CO selectively. This finding not only elucidates the reaction mechanisms for the photocatalytic CO₂ reduction but also leads us to design more effective metal complexes for the catalyses.

Acknowledgements

This work was supported by the PRESTO Program of JST. We thank Mr Masaya Kamiya and Mr Kousuke Matsuura for experimental supports.

References and Notes

- 1 G. A. Olah, G. K. S. Prakash and A. Goepfert, *J. Am. Chem. Soc.*, 2011, **133**, 12881–12898.
- 2 T. R. Cook, D. K. Dogutan, S. Y. Reece, Y. Surendranath, T. S. Teets and D. G. Nocera, *Chem. Rev.*, 2010, **110**, 6474–6502.
- 3 J. H. Alstrum-Acevedo, M. K. Brennaman and T. J. Meyer, *Inorg. Chem.*, 2005, **44**, 6802–6827.
- 4 H. Arakawa, M. Aresta, J. N. Armor, M. A. Barteau, E. J. Beckman, A. T. Bell, J. E. Bercaw, C. Creutz, E. Dinjus, D. A. Dixon, K. Domen, D. L. DuBois, J. Eckert, E. Fujita, D. H. Gibson, W. A. Goddard, D. W. Goodman, J. Keller, G. J. Kubas, H. H. Kung, J. E. Lyons, L. E. Manzer, T. J. Marks, K. Morokuma, K. M. Nicholas, R. Periana, L. Que, J. Rostrup-Nielson, W. M. H. Sachtler, L. D. Schmidt, A. Sen, G. A. Somorjai, P. C. Stair, B. R. Stults and W. Tumas, *Chem. Rev.*, 2001, **101**, 953–996.
- 5 K. Kobayashi and K. Tanaka, *Phys. Chem. Chem. Phys.*, 2014, **16**, 2240–2250.
- 6 D. L. DuBois, *Inorg. Chem.*, 2014, **53**, 3955–3960.
- 7 A. M. Appel, J. E. Bercaw, A. B. Bocarsly, H. Dobbek, D. L. DuBois, M. Dupuis, J. G. Ferry, E. Fujita, R. Hille, P. J. A. Kenis, C. A. Kerfeld, R. H. Morris, C. H. F. Peden, A. R. Portis, S. W. Ragsdale, T. B. Rauchfuss, J. N. H. Reek, L. C. Seefeldt, R. K. Thauer and G. L. Waldrop, *Chem. Rev.*, 2013, **113**, 6621–6658.
- 8 C. D. Windle and R. N. Perutz, *Coord. Chem. Rev.*, 2012, **256**, 2562–2570.
- 9 T. Yui, Y. Tamaki, K. Sekizawa and O. Ishitani, *Top. Curr. Chem.*, 2011, **303**, 151–184.
- 10 H. Takeda and O. Ishitani, *Coord. Chem. Rev.*, 2010, **254**, 346–354.
- 11 K. Tanaka, *Chem. Rec.*, 2009, **9**, 169–186.
- 12 A. J. Morris, G. J. Meyer and E. Fujita, *Acc. Chem. Res.*, 2009, **42**, 1983–1994.
- 13 E. E. Benson, C. P. Kubiak, A. J. Sathrum and J. M. Smieja, *Chem. Soc. Rev.*, 2009, **38**, 89–99.
- 14 J.-M. Savéant, *Chem. Rev.*, 2008, **108**, 2348–2378.



- 15 P. G. Jessop, T. Ikariya and R. Noyori, *Chem. Rev.*, 1995, **95**, 259–272.
- 16 M. D. Sampson, A. D. Nguyen, K. A. Grice, C. E. Moore, A. L. Rheingold and C. P. Kubiak, *J. Am. Chem. Soc.*, 2014, **136**, 5460–5471.
- 17 H. Takeda, H. Koizumi, K. Okamoto and O. Ishitani, *Chem. Commun.*, 2014, **50**, 1491–1493.
- 18 M. Bourrez, F. Molton, S. Chardon-Noblat and A. Deronzier, *Angew. Chem., Int. Ed.*, 2011, **50**, 9903–9906.
- 19 C. Costentin, S. Drouet, M. Robert and J.-M. Savéant, *Science*, 2012, **338**, 90–94.
- 20 J. Grodkowski, D. Behar, P. Neta and P. Hambright, *J. Phys. Chem. A*, 1997, **101**, 248–254.
- 21 M. Hammouche, D. Lexa, M. Momenteau and J.-M. Savéant, *J. Am. Chem. Soc.*, 1991, **113**, 8455–8466.
- 22 R. Ziessel, J. Hawecker and J.-M. Lehn, *Helv. Chim. Acta*, 1986, **69**, 1065–1084.
- 23 S. Matsuoka, K. Yamamoto, T. Ogata, M. Kusaba, N. Nakashima, E. Fujita and S. Yanagida, *J. Am. Chem. Soc.*, 1993, **115**, 601–609.
- 24 A. H. P. Tinnemans, T. P. M. Koster, D. H. M. W. Thewissen and A. Mackor, *Recl. Trav. Chim. Pays-Bas*, 1984, **103**, 288–295.
- 25 M. Rudolph, S. Dautz and E.-G. Jäger, *J. Am. Chem. Soc.*, 2000, **122**, 10821–10830.
- 26 M. A. Mndez, P. Voyame and H. H. Girault, *Angew. Chem., Int. Ed.*, 2011, **50**, 7391–7394.
- 27 J. L. Grant, K. Goswami, L. O. Spreer, J. W. Otvos and M. Calvin, *J. Chem. Soc., Dalton Trans.*, 1996, 2581–2583.
- 28 M. L. Clark, K. A. Grice, C. E. Moore, A. L. Rheingold and C. P. Kubiak, *Chem. Sci.*, 2014, **5**, 1894–1900.
- 29 S. C. Rasmussen, M. M. Richter, E. Yi, H. Place and K. J. Brewer, *Inorg. Chem.*, 1990, **29**, 3926–3932.
- 30 C. M. Bolinger, N. Story, B. P. Sullivan and T. J. Meyer, *Inorg. Chem.*, 1988, **27**, 4582–4587.
- 31 P. R. Bernatis, A. Miedaner, R. C. Haltiwanger and D. L. DuBois, *Organometallics*, 1994, **13**, 4835–4843.
- 32 D. L. DuBois, A. Miedaner and R. C. Haltiwanger, *J. Am. Chem. Soc.*, 1991, **113**, 8153–8164.
- 33 D. L. DuBois and A. Miedaner, *J. Am. Chem. Soc.*, 1987, **109**, 113–117.
- 34 Y. Kou, Y. Nabetani, D. Masui, T. Shimada, S. Takagi, H. Tachibana and H. Inoue, *J. Am. Chem. Soc.*, 2014, **136**, 6021–6030.
- 35 T. Morimoto, T. Nakajima, S. Sawa, R. Nakanishi, D. Imori and O. Ishitani, *J. Am. Chem. Soc.*, 2013, **135**, 16825–16828.
- 36 T. Morimoto, C. Nishiura, M. Tanaka, J. Rohacova, Y. Nakagawa, Y. Funada, K. Koike, Y. Yamamoto, S. Shishido, T. Kojima, T. Saeki, T. Ozeki and O. Ishitani, *J. Am. Chem. Soc.*, 2013, **135**, 13266–13269.
- 37 Y. Tamaki, K. Koike, T. Morimoto, Y. Yamazaki and O. Ishitani, *Inorg. Chem.*, 2013, **52**, 11902–11909.
- 38 Y. Tamaki, K. Koike, T. Morimoto and O. Ishitani, *J. Catal.*, 2013, **304**, 22–28.
- 39 H. Takeda, K. Koike, H. Inoue and O. Ishitani, *J. Am. Chem. Soc.*, 2008, **130**, 2023–2031.
- 40 B. Gholamkhash, H. Mametsuka, K. Koike, T. Tanabe, M. Furue and O. Ishitani, *Inorg. Chem.*, 2005, **44**, 2326–2336.
- 41 Y. Hayashi, S. Kita, B. S. Brunshwig and E. Fujita, *J. Am. Chem. Soc.*, 2003, **125**, 11976–11987.
- 42 J. Hawecker, J.-M. Lehn and R. Ziessel, *Helv. Chim. Acta*, 1986, **69**, 1990–2012.
- 43 J. Chauvin, F. Lafolet, S. Chardon-Noblat, A. Deronzier, M. Jakonen and M. Haukka, *Chem.–Eur. J.*, 2011, **17**, 4313–4322.
- 44 M. R. M. Bruce, E. Megehee, B. P. Sullivan, H. H. Thorp, T. R. O'Toole, A. Downard, J. R. Pug and T. J. Meyer, *Inorg. Chem.*, 1992, **31**, 4864–4873.
- 45 S. Sato, T. Morikawa, T. Kajino and O. Ishitani, *Angew. Chem., Int. Ed.*, 2013, **52**, 988–992.
- 46 P. Kang, C. Cheng, Z. Chen, C. K. Schauer, T. J. Meyer and M. Brookhart, *J. Am. Chem. Soc.*, 2012, **134**, 5500–5503.
- 47 Y. Kuramochi, M. Kamiya and H. Ishida, *Inorg. Chem.*, 2014, **53**, 3326–3332.
- 48 P. Voyame, K. E. Toghil, M. A. Méndez and H. H. Girault, *Inorg. Chem.*, 2013, **52**, 10949–10957.
- 49 Y. Tamaki, T. Morimoto, K. Koike and O. Ishitani, *Proc. Natl. Acad. Sci. U. S. A.*, 2012, **109**, 15673–15678.
- 50 J. R. Pugh, M. R. M. Bruce, B. P. Sullivan and T. J. Meyer, *Inorg. Chem.*, 1991, **30**, 86–91.
- 51 H. Ishida, T. Terada, K. Tanaka and T. Tanaka, *Inorg. Chem.*, 1990, **29**, 905–911.
- 52 H. Ishida, K. Tanaka and T. Tanaka, *Chem. Lett.*, 1988, 339–342.
- 53 H. Ishida, K. Tanaka and T. Tanaka, *Chem. Lett.*, 1987, 1035–1038.
- 54 H. Ishida, H. Tanaka, K. Tanaka and T. Tanaka, *J. Chem. Soc., Chem. Commun.*, 1987, 131–132.
- 55 H. Ishida, K. Tanaka and T. Tanaka, *Organometallics*, 1987, **6**, 181–186.
- 56 H. Ishida, K. Tanaka and T. Tanaka, *Chem. Lett.*, 1985, 405–406.
- 57 J. Hawecker, J.-M. Lehn and R. Ziessel, *J. Chem. Soc., Chem. Commun.*, 1985, 56–58.
- 58 K. Maeda, K. Sekizawa and O. Ishitani, *Chem. Commun.*, 2013, **49**, 10127–10129.
- 59 T. M. Suzuki, H. Tanaka, T. Morikawa, M. Iwaki, S. Sato, S. Saeki, M. Inoue, T. Kajino and T. Motohiro, *Chem. Commun.*, 2011, **47**, 8673–8675.
- 60 S. Sato, T. Arai, T. Morikawa, K. Uemura, T. M. Suzuki, H. Tanaka and T. Kajino, *J. Am. Chem. Soc.*, 2011, **133**, 15240–15243.
- 61 T. Arai, S. Sato, K. Uemura, T. Morikawa, T. Kajino and T. Motohiro, *Chem. Commun.*, 2010, **46**, 6944–6946.
- 62 S. Sato, T. Morikawa, S. Saeki, T. Kajino and T. Motohiro, *Angew. Chem., Int. Ed.*, 2010, **49**, 5101–5105.
- 63 (a) S. Chardon-Noblat, C. H. Cripps, A. Deronzier, J. S. Field, S. Gouws, R. J. Haines and F. Southway, *Organometallics*, 2001, **20**, 1668–1675; (b) S. Chardon-Noblat, C. P. Da, A. Deronzier, M. Haukka, T. A. Pakkanen and R. Ziessel, *J. Electroanal. Chem.*, 2000, **490**, 62–69.
- 64 S. Chardon-Noblat, A. Deronzier, R. Ziessel and D. Zsoldos, *J. Electroanal. Chem.*, 1998, **444**, 253–260.



- 65 S. Chardon-Noblat, A. Deronzier, R. Ziessel and D. Zsoldos, *Inorg. Chem.*, 1997, **36**, 5384–5389.
- 66 S. Chardon-Noblat, M. N. Collomb-Dunand-Sauthier, A. Deronzier, R. Ziessel and D. Zsoldos, *Inorg. Chem.*, 1994, **33**, 4410–4412.
- 67 M. N. Collomb-Dunand-Sauthier, A. Deronzier and R. Ziessel, *Inorg. Chem.*, 1994, **33**, 2961–2967.
- 68 M. N. Collomb-Dunand-Sauthier, A. Deronzier and R. Ziessel, *J. Chem. Soc., Chem. Commun.*, 1994, 189–191.
- 69 H. Ishida, K. Fujiki, T. Ohba, K. Ohkubo, K. Tanaka, T. Terada and T. Tanaka, *J. Chem. Soc., Dalton Trans.*, 1990, 2155–2160.
- 70 J.-M. Lehn and R. Ziessel, *J. Organomet. Chem.*, 1990, **382**, 157–173.
- 71 S. Chardon-Noblat, A. Deronzier, D. Zsoldos, R. Ziessel, M. Haukka, T. Pakkanen and T. Venalainen, *J. Chem. Soc., Dalton Trans.*, 1996, 2581–2583.
- 72 S. Myllynen and M. Wasberg, *J. Electroanal. Chem.*, 2008, **623**, 93–101.
- 73 M. Haukka, J. Kiviaho, M. Ahlgren and T. A. Pakkanen, *Organometallics*, 1995, **14**, 825–833.
- 74 A. Paul, D. Connolly, M. Schulz, M. T. Pryce and J. G. Vos, *Inorg. Chem.*, 2012, **51**, 1977–1979.
- 75 P. A. Anderson, G. B. Deacon, K. H. Haarmann, F. R. Keene, T. J. Meyer, D. A. Reitsma, B. W. Skelton, G. F. Strouse, N. C. Thomas, J. A. Treadway and A. H. Whit, *Inorg. Chem.*, 1995, **34**, 6145–6157.
- 76 K. Suzuki, A. Kobayashi, S. Kaneko, K. Takehira, T. Yoshihara, H. Ishida, Y. Shiina, S. Oishi and S. Tobita, *Phys. Chem. Chem. Phys.*, 2009, **11**, 9850–9860.
- 77 M. Schmittel, A. Ganz, W. A. Schenk and M. Z. Hagel, *Z. Naturforsch., B: J. Chem. Sci.*, 1999, **54**, 559–564.
- 78 D. Mauzerall and F. H. Westheimer, *J. Am. Chem. Soc.*, 1955, **77**, 2261–2264.
- 79 M. N. Collomb-Dunand-Sauthier, A. Deronzier and R. Ziessel, *J. Electroanal. Chem.*, 1991, **319**, 347–353.
- 80 M. N. Collomb-Dunand-Sauthier, A. Deronzier and R. Ziessel, *J. Electroanal. Chem.*, 1993, **350**, 43–55.
- 81 G. J. Kavarnos, *Fundamentals of Photoinduced Electron Transfer*, Wiley-VCH, Weinheim, 1993.
- 82 M. Z. Hoffman, *J. Phys. Chem.*, 1988, **92**, 3458–3464.
- 83 E. Fujita, M. Chou and K. Tanaka, *Appl. Organomet. Chem.*, 2000, **14**, 844–846.
- 84 Y. Kuramochi, Y. Ito and H. Ishida, *Eur. J. Inorg. Chem.*, 2012, **2012**, 1167–1170.
- 85 The quenching rate constant was estimated by using the Stern–Volmer constant of $K_{SV} = 13 \text{ M}^{-1}$ (Fig. S5†) and the emission lifetime of $[\text{Ru}(\text{4dmbpy})_3]^2$, assumed to be 766 ns. See ref. 49.
- 86 S. Myllynen, M. Wasberg and M. Haukka, *J. Electroanal. Chem.*, 2006, **586**, 217–224.
- 87 We have also examined the photochemical CO_2 reduction catalysed by *trans*(Cl)–Ru(4dmbpy)(CO)₂Cl₂, whose first reduction potential is $-1.58 \text{ V vs. Ag/Ag}^+$ in DMA/water (9 : 1 v/v). The dependence of the product selectivity on the catalyst concentration is similar to that of *trans*(Cl)–Ru(bpy)(CO)₂Cl₂, eliminating the possibility that the simple electric effect of the substituents changes the product selectivity.

